journal

J. Am. Ceram. Soc., 79 [5] 1377–88 (1996)

Computer Simulations of Binder Removal from 2-D and 3-D Model Particulate Bodies

Jennifer A. Lewis* and Michael A. Galler

Department of Materials Science and Engineering and the Beckman Institute of Advanced Science and Technology, University of Illinois, Urbana, Illinois 61801

Dale P. Bentz*

National Institute of Standards and Technology,† Gaithersburg, Maryland 20899

A series of computer simulations were developed to investigate the removal of multicomponent, thermoplastic binders from two- and three-dimensional model particulate bodies. Monosized particles with varying diameters were randomly placed in such systems, and all unoccupied pixels were assigned to the binder phase at ratios of 1:9, 1:2, or 1:1 plasticizer (volatile) to polymeric (nonvolatile) species. Simulations were carried out under isothermal conditions to study the influence of liquid-phase transport processes, i.e., plasticizer diffusion in the binder-filled pore network and capillary-driven redistribution of the binder phase, on plasticizer removal rates. Plasticizer diffusion was modeled by a random-walk algorithm, and nonplanar pore development arising from capillary-driven binder redistribution was modeled by an invasion percolation algorithm. For comparison, simulations were also carried out on systems in which binder redistribution was not permitted. In such cases, pore development was modeled as an advancing or nonadvancing planar front. Visualization of transport phenomena on a microscopic scale has provided the first quantitative assessment of plasticizer concentration profiles, $C(t)$ and $C(z)$, and binder–vapor interfacial development during removal. Removal rates were significantly enhanced when capillary-driven binder redistribution was assumed, and they depended strongly on initial plasticizer content under those conditions.

I. Introduction

MULTICOMPONENT organic binder systems, such as plasticized-thermoplastic polymers, are widely used ceramics processing aids. Polymeric species serve many functions, including (1) modifying the rheological behavior of suspensions and pastes of ceramic particles, (2) "binding" individual particles together to impart green strength, and (3) enabling the lamination of ceramic thick films. Low-molecular-weight plasticizing species serve mainly to modify the polymer's glass transition temperature and, hence, its viscoelastic properties at a given temperature.[1] Ceramic fabrication techniques utilize these processing aids to varying extents. For example, components fabricated by injection molding or tape casting can contain an appreciable amount of organic (≈30–40 vol% of the component). In such cases, the binder phase nearly or completely fills the void space between densely packed ceramic particles.[2,3] These components are referred to as *closed-pore compacts*. In contrast, components fabricated by cold isostatic pressing or dry pressing contain relatively little organic binder (≈5–10 vol% of the component). These components are *open-pore compacts*, which contain interconnected pore channels in the as-formed state.

Organic processing aids are transient additives that must be eliminated from ceramic components prior to densification without introducing strength-limiting defects (e.g., large voids, cracks, or delamination). Thus, binder removal (or debinding) is a critical processing step in the production of advanced ceramics. Often it is also the slowest processing step, particularly for injection-molded components.[4] Several debinding schemes have been proposed including (1) solvent extraction, (2) wicking, and (3) thermal decomposition. Thermal debinding is most viable for high-volume production and, hence, is favored by the ceramics industry.

Multicomponent binders can be classified as graded-volatility systems, because only the low-molecular-weight plasticizing species have an appreciable vapor pressure below the decomposition temperature, T_d, of the polymer. Such volatility differences are exploited by two-stage thermal debinding cycles, where plasticizers are eliminated during the first stage, followed by the removal of polymer decomposition products at higher temperatures during the second stage. In the temperature range $T < T_d$, organic species can be separated into volatile and nonvolatile elements, where only the volatile species (e.g., plasticizers and residual solvent) can evaporate. Volatile species are initially distributed within the ceramic component at some concentration and must diffuse through binder-filled pores to the binder–vapor interface, where evaporation occurs. Nonvolatile (polymeric) species must undergo degradation to produce volatile decomposition products (e.g., monomers, dimers, CO_2, H_2O) at temperatures above T_d. These species must also diffuse to the binder–vapor interface to evaporate. The generation rate of volatile products must be balanced with their removal rate to minimize defect formation, which may occur when the local concentration of such species exceeds that in equilibrium with the vapor at $P = 1$ atm.[5–7] This delicate balance, however, is difficult to achieve because of the narrow temperature range and exothermic nature of many polymer degradation processes. One anticipated benefit of a two-stage debinding cycle is that the porosity developed during the first stage will facilitate the subsequent removal of these decomposition products during the later stage.

To aid the design of improved thermoplastic binder systems and removal conditions, a fundamental understanding is required of the physical and chemical processes that occur during thermal debinding, e.g., mass and heat transport, binder

D. J. Shanefield—contributing editor

Manuscript No. 192847. Received February 9, 1995; approved November 29, 1995.
*Member, American Ceramic Society.
†Building Materials Division, Building and Fire Research Laboratory, Technology Administration, U.S. Department of Commerce.

distribution processes, polymer degradation mechanisms, and associated ceramic surface interactions. In recent years, several simple quantitative models have been proposed which focus on the governing mass transport mechanisms during binder removal.[4,7-10] For example, German[8] investigated the influence of two controlling processes during thermal debinding of closed-pore, injection-molded components: pressure-driven gas diffusion and permeation. In his work, the diffusion of organic species within the binder phase, as well as capillary-driven liquid transport processes were neglected. The binder–vapor interface was modeled as a planar front, which receded into the compact as removal progressed. The development of penetrating pore channels (or fingering) was ignored, as it was assumed that such effects did not greatly alter the total debinding time. These models were applied to study the removal of a single-component, ideal binder system (viz., water) which did not undergo thermal decomposition. The effects of particle size, porosity, and component size on debinding times were assessed.

In a series of papers, Cima and Lewis[5,9-11] demonstrated that capillary-driven liquid-phase transport plays an important role in the thermal debinding of closed-pore, tape-cast ceramic layers, which contain a two-component, thermoplastic binder system. They reported the development of a nonplanar pore front (or binder–vapor interface) as removal progressed,[9] and directly observed such processes in two-dimensional binder-filled pore networks.[5] Based on their experimental observations, a model was proposed to determine the contribution of capillary-driven liquid transport based on parameters associated with the binder system, particle bed, and removal conditions.[9] Through additional experiments, they demonstrated that the diffusion of organic species in the binder (or liquid) phase was the rate-limiting process for isothermal plasticizer removal from these ceramic layers, and that capillary-driven binder redistribution accelerated their removal.[10] The enhanced plasticizer removal rates were largely attributed to the reduction in the characteristic diffusion length resulting from capillary-driven liquid transport. In this situation, the length scale no longer depends on the component dimensions, but rather on the distance between large, penetrating empty pores (which is of the order of several particle diameters). Additional support for the importance of these mass transport mechanisms was recently reported by Angermann and co-workers.[12,13] They studied the thermal debinding of injection-molded components which contained a two-component binder system, and found that removal of low-molecular-weight species was governed by diffusion in the polymer phase. Invoking the analysis of Lewis and Cima,[10] they estimated characteristic diffusion lengths of several particle diameters, suggesting that capillary-driven binder redistribution also occurred in their debinding process. Barone and Ulciny[4] have also studied liquid-phase transport during the removal of organic binders from closed-pore, injection-molded ceramic components. They developed a model to evaluate the relative importance of capillary-driven liquid-phase transport and gas-phase transport during thermal debinding. Their model was first applied to study the removal of a single-component, nondegradable binder system, and then extended to account for polymer degradation processes. A key conclusion of their work was that liquid-phase transport processes dominate throughout most of the debinding cycle for closed-pore compacts.

In this paper, we utilize computer modeling as an ancillary tool to further investigate the importance of liquid-phase transport phenomena, including diffusion of volatile species in the binder phase and capillary-driven binder redistribution processes, during thermal debinding. A series of two-dimensional (2-D) and three-dimensional (3-D) computer simulations have been developed to study the effects of binder composition (e.g., plasticizer content), pore development, and component properties (e.g., particle size) on removal kinetics. Given the complexity of the binder removal process, we have chosen to address only the isothermal removal of plasticizer species from closed-pore bodies which contain two-component binder systems comprised of volatile and nonvolatile elements in the first generation of these simulations. The first computer simulation, a nonplanar model, combines two algorithms: (1) a random-walk algo-rithm[14-19] that simulates volatile plasticizer diffusion in binder-filled pores, and (2) an invasion percolation algorithm[20-24] that simulates capillary-driven binder redistribution processes. Though these algorithms have been utilized separately in previous work, to our knowledge this is the first computer model where invasion percolation is coupled to a diffusion-controlled mass transport process. In this model, a nonplanar pore front develops, as the removal of volatile species progresses and the remaining binder is redistributed within the pore network via capillary forces. For comparison, two other computer simulation models, the planar and no-intrusion models, have also been developed which account for volatile diffusion, but differ in pore development from the nonplanar model by allowing for either planar or no-pore development, respectively. Though less physically realistic, these models serve as benchmarks in this work.

The computer simulation models offer several advantages over analytical approaches that describe the system by a set of differential equations relating the flux of the diffusing species to the local concentration gradients and component geometry based on Fick's first and second laws of diffusion.[25,26] First, computer simulations allow one to readily visualize the processes being modeled. Second, analytical approaches have limited accuracy in describing the interactions between diffusing species and individual ceramic particles and in accounting for changes in boundary conditions when the pore development (or binder–vapor interface) is nonplanar. The first limitation can be addressed by empirically adjusting the diffusion coefficient to account for the binder fraction and tortuous pore network present in the ceramic body.[10,27] However, in our approach, the tortuous nature of a given system can be directly assessed using the no-intrusion model. The second limitation arises because of the complex, random nature of the nonplanar binder–vapor interface relative to planar pore and no-intrusion fronts. Again, the growth of this nonplanar interface can be quantified using our approach. Ultimately, we plan to execute these models on digitized images of the cross sections of real ceramic components as well as to incorporate added complexity, such as polymer (nonvolatile) degradation and gas transport processes.

II. Description of Computer Simulations

Three computer simulation models were developed in this investigation as introduced above: (1) the nonplanar model, (2) the planar model, and (3) the no-intrusion model. Each model incorporated a random-walk algorithm and, when needed, an additional algorithm to simulate their respective pore development processes. These models were executed on both 2-D and 3-D particulate systems generated using the methods described below. To minimize system size effects, the results obtained from simulations carried out using a given set of conditions were averaged over more than 10 realizations unless otherwise noted.

(1) 2-D System Generation

The 2-D particulate systems were modeled by a rectangular array of pixels (width (X) $\times$ depth (Z), where X = 400 or 800 pixels, and Z = 200, 400, 600, or 800 pixels) defined such that each pixel initially represented either the ceramic (solid) or the organic binder phase. Several systems were generated containing monosized ceramic particles with diameters (PD) between 13 and 31 pixels. These circular particles were formed by first centering a continuum circle on a given pixel (defined by x, z coordinates) and then changing all pixels whose centers fell within the boundary of the continuum circle to the solid phase as shown in Fig. 1.[28] Particulate bodies were constructed

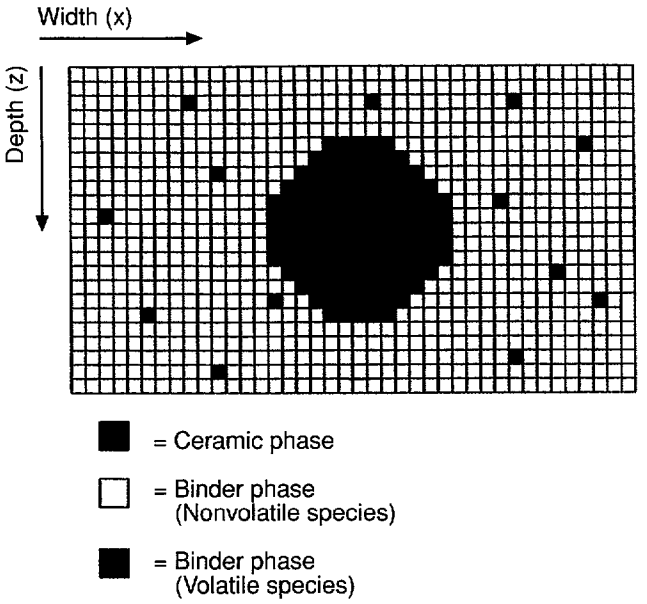

Fig. 1. Schematic view of an individual ceramic particle (diameter, PD = 13 pixels) in the 2-D model system. (Note: The pixels surrounding the particle have been assigned to the binder phase as either volatile or nonvolatile species.)

by randomly placing many such nonoverlapping circles on a given rectangular unit cell. Periodic boundary conditions were employed during particle placement to eliminate edge effects so that any portion of a circular particle which extended beyond the rectangular boundaries was translated into the rectangle on the opposite side.

All 2-D systems contained 53% solid particles with 47% binder phase filling the remaining (pore) space between individual particles. Note that this value is just above the minimum pore content of 45% achievable for parking of monosized circles, referred to as the "random parking limit."[28] A fraction of the pixels representing the binder phase were then randomly assigned to be volatile, plasticizer species, such that each of these pixels represents an individual plasticizer molecule (refer to Fig. 1). One can scale these systems to actual distances by assigning a unit distance to each side of a pixel. For example, if one chooses a distance of 10 nm/side, then reasonable values for the respective sizes of the organic (D = 10 nm) and ceramic (PD = 130–310 nm) phases are obtained. Note, a diameter of several nanometers may exhibit reasonable agreement with the characteristic dimensions of individual polymeric coils, but overestimates the size of most low-molecular-weight plasticizers.[29] Three binder systems were generated in these simulations with volatile concentrations of 10%, 33%, and 50% of the total binder phase corresponding to a plasticizer (volatile) to polymer (nonvolatile) ratios of 9:1, 2:1, and 1:1, respectively. Such plasticizer concentrations are representative of those used in many commercial binder systems (e.g., see Ref. 3).

(2) 3-D System Generation

The 3-D particulate systems were modeled by an array of pixels (width (X) × length (Y) × depth (Z), where X, Y = 400 pixels, and Z = 200 pixels) defined such that each pixel initially represented either the ceramic (solid) or the organic binder phase. Systems were generated containing monosized ceramic particles with diameters (PD) of 13 pixels. The box used for particle placement has periodic x, y (horizontal) dimensions equal to those of the 3-D model system, with an extended z (vertical) dimension of nine particle diameters—four particle diameters above the actual top surface (z = 0 pixels) of the 3-D system, and five particle diameters below its bottom surface (z = 200 pixels)—to eliminate edge effects during particle placement.[30] A spherical particle is placed by choosing a random coordinate for its center in the x–y plane at a height of one particle radius above the top of the highest previously placed particle or, in the absence of placed particles, the extended bottom surface. The particle is allowed to fall until it hits either another particle or the extended bottom surface. Upon hitting this bottom surface, the particle is placed in that location. If the particle hits a previously placed particle, then its vertical motion ceases, and the particle attempts to move 1 pixel in a randomly chosen direction in the x–y plane. If the move is successful, the particle attempts to resume downward movement. If the move is unsuccessful (i.e., another particle blocks its movement), then another direction is randomly chosen and similarly tested. If all eight directions are blocked (i.e., nearest-neighbor and second-nearest-neighbor locations), then this process is repeated at a distance of 2, then 3, and 4 pixels. If movement is still not possible, the particle is considered "trapped" and placed in that location. New particles are then placed following this same procedure until 36 particles are consecutively placed so that they lie completely above the top boundary of the normal simulation volume (defined as the 3-D system). Note, particles are never permitted to overlap at any point during the placement process.

Unlike the 2-D systems, the 3-D systems are mechanically stable because of the differences in their respective particle placement algorithms. All 3-D systems contained approximately 57% solid particles with 43% binder phase filling the remaining (pore) space between individual particles. A fraction of the pixels representing the binder phase were then randomly assigned to be volatile (plasticizer) species such that each pixel is equivalent to an individual plasticizer molecule (refer to Fig. 1). Two binder systems with plasticizer (volatile) contents of 33% or 50% of the total binder phase (i.e., 2:1 or 1:1 nonvolatile:volatile species) were studied in these simulations.

(3) Random-Walk Algorithm

King[14] was first to suggest the application of the Monte Carlo (MC) method to diffusion problems. Subsequently, several investigators have successfully employed this technique to study various relevant diffusion problems.[14–19] In this work, a random-walk algorithm was used to simulate the diffusion of volatile species in the binder phase within the model particulate systems described above. This process is assumed to occur under isothermal conditions below the decomposition temperature of the polymer (i.e., the nonvolatile component of binder phase). The volatile species conduct random walks analogous to Brownian motion within the binder-filled pores, where each new jump (or step) is independent of the previous one. In a given time step, all volatile species in the system have an opportunity to execute a one-step random walk (distance = 1 pixel) in one of four directions ($\pm x, \pm z$) in the 2-D systems or one of six directions ($\pm x, \pm y, \pm z$) in the 3-D systems. Each direction has an equal probability of being selected,[14] but not all jumps are allowed. For example, volatile species are reflected back to their original positions when attempting to jump onto a pixel occupied by the ceramic phase. At the system boundaries, their interactions are as follows: Volatile species are reflected back to their original positions when attempting to jump across the bottom boundary. Periodic boundary conditions are employed at the side boundaries to avoid edge effects. Finally, volatile species are removed from the system when attempting to jump across the top surface, or binder–vapor interface. The total number of volatile species remaining in the system at each time step was recorded during the simulations. At intermittent time steps, the number of volatile species at a given depth (z) in the system was also recorded.

(4) Nonplanar Pore Development (Invasion) Algorithm

Wilkinson and Willemsen[20] developed a new form of percolation theory,[22] referred to as invasion percolation, that explic-

itly accounts for the transport processes dominated by capillary forces that occur in random porous media. Invasion percolation is based on the dynamic advance of the interface between two fluids, a nonwetting fluid and a wetting fluid, where the advance occurs at the point of least resistance, as opposed to the case where the entire interface advances up to some threshold resistance. The pressure difference between the fluids (i.e., the capillary pressure) is given by

$$P_{\text{invading fluid}} - P_{\text{displaced fluid}} = \frac{2\gamma \cos \theta}{r} \quad (1)$$

where, in this case, γ is the surface tension of the binder–vapor interface, θ is the contact angle between this interface and the pore wall, and r is the pore radius.[31] Invasion percolation theory has been utilized to understand drying phenomena in particulate beds[23] and to model oil recovery processes.[20] The similarity between thermoplastic binder thermolysis and drying[9] permits the use of an invasion algorithm to simulate the development of a nonplanar pore front (or binder–vapor interface) during removal. In this case, the invading vapor phase, a nonwetting fluid, displaces the binder phase, a wetting fluid, as volatile species are eliminated from the system.

We have modified an algorithm for nonwetting fluid invasion developed by Garboczi and Bentz,[24] which is a geometric method accurate for completely nonwetting ($\theta = 180°$) fluid injection in two dimensions. The development of the binder–vapor interface is controlled by a mass balance with the number of volatile species exiting the system. Given the substantial differences in plasticizer diffusivities between binder-filled (i.e., 10^{-6}–10^{-10} cm^2/s) and empty pores ($\approx 10^{-2}$/s) in real components[10] and the results of Barone and Ulciny,[4] it is assumed that volatile species are immediately removed from the system once they have reached this penetrating binder–vapor interface. Thus, gas-phase transport processes are neglected in this work. It is also assumed that viscous forces are negligible compared to capillary forces for this process, implying that the binder phase can instantaneously redistribute within the pore network of these systems.

To locate the initial point of least resistance for pore (or binder–vapor interface) advancement, the maximum diameter of the binder-filled pores connected to the top boundary ($z = 0$) was first assessed by finding which of these pores could accommodate a circle (2-D) or sphere (3-D) of the largest diameter. The number of pixels required to advance the binder–vapor interface into this largest pore diameter was then determined for each system. Once this value was found, the removal process was initiated. Once the requisite number of volatile species were eliminated from the system via diffusion to this interface, the vapor (nonwetting) phase was advanced in a circular (2-D) or spherical (3-D) intruding shape giving an approximation to the expected catenoid meniscus. Following each binder–vapor interface advancement, all binder-filled pores in contact with the vapor phase were again reassessed to find the new location of the maximum intrudable pore diameter. This iterative process was carried out until approximately all the volatile species were eliminated from the system. Note that a small fraction of the initial volatile species can remain trapped in binder-filled pores that are isolated (or disconnected) from the continuous pore network in these systems.

The initial length (2-D) or surface area (3-D) of the binder–vapor interface, $A_{\text{int}}(0)$, was determined by counting all binder pixels at the top boundary of each system. As removal progressed, the length (or area) of this interface, $A_{\text{int}}(t)$, was reassessed at intermittent times during the simulations. In 2-D systems, this was achieved using an "effective length" algorithm which summed all appropriate pixels that remained at the top surface of the system as well as those along the penetrating binder–vapor interface at a given time. The binder-filled pixels along the top surface of the system were assigned a value of one pixel for their interfacial length. Interior pixels have four nearest neighbors ($\pm x$ and $\pm z$), and those at the binder–vapor interface can have one of two neighbor configurations. In the first configuration, a binder-filled pixel at the interface is surrounded by two binder-filled pixels and two pore pixels and a value of 1.296 pixels ($=(\sqrt{2} + 3/8\pi)/2$) is used to define their length. This value was assigned as an approximation of the actual curved surface, to minimize errors associated with measuring interfacial length in a pixelated system. In the second configuration, this binder-filled interior pixel is surrounded by three binder-filled pixels and one pore pixel. In this case, a value of one pixel was used to define their contribution to the interfacial length. For an intruding pore whose diameter (D_{pore}) equals 21 pixels, this algorithm would calculate an interfacial length that is approximately 5.5% lower than the actual pore perimeter ($=0.5\pi D_{\text{pore}}$). In 3-D systems, the surface area of the binder–vapor interface was determined by summing the number of pixel faces in which vapor-phase pixels were adjacent to the binder phase. The six nearest-neighbor positions of a given vapor-phase pixel were assessed to locate such binder-phase pixels. In addition, the total number of pixel faces associated with binder-phase pixels at the top surface at a given time were also included in this count.

(5) Planar Pore Development Algorithm

Planar pore development requires that the binder–vapor interface remains flat as removal progresses. This type of interface may develop for systems with a fixed number of volatile species whose size was much less than one pixel. A planar interface may also realistically develop when the volatile removal rate is much larger than the rate at which the remaining binder phase can redistribute within the porous network, for a binder phase comprised of 100% volatile species. In the planar model, pore development advances uniformly into the model particulate systems at discrete depth intervals of one pixel. The initial binder–vapor interface is defined by the top boundary ($z = 0$) of the 2-D and 3-D systems. The number of binder pixels at this boundary was first assessed, and then removal was initiated. Analogous to the nonplanar pore development algorithm, volatile species were removed from the system once they reached the penetrating binder–vapor interface. When the appropriate number of volatile species was eliminated from the system, the binder–vapor interface was allowed to advance a depth (z) of one pixel to conserve mass within the system. The number of binder pixels along the interface was then reassessed. The binder–vapor interface was again allowed to advance once the appropriate number of volatile species had been removed. This iterative process was repeated until all volatile species were eliminated from the system.

(6) No-Intrusion Algorithm

The no-intrusion algorithm is employed to model mass transport processes that occur far away from the binder–vapor interface, and thus is useful for distinguishing interactions between diffusing species and individual solid particles in these systems. In the no-intrusion model, pixels initially assigned as volatile species are reassigned to the nonvolatile phase, once these species are eliminated from the system. Thus, the binder–vapor interface remains at the top surface ($z = 0$) throughout each simulation.

III. Results

(1) 2-D Simulations

The normalized plasticizer concentration ($C(t)/C_0$) is plotted as a function of removal time in Fig. 2 for 2-D model systems (400×200 pixels, PD = 13 pixels) with varying binder composition, where $C(t)$ equals the total number of plasticizer species in the system at a given time, t, and C_0 equals the initial number of plasticizer species in the system. These curves correspond to isothermal mass loss profiles for binder removal at some temperature below the decomposition temperature of the poly-

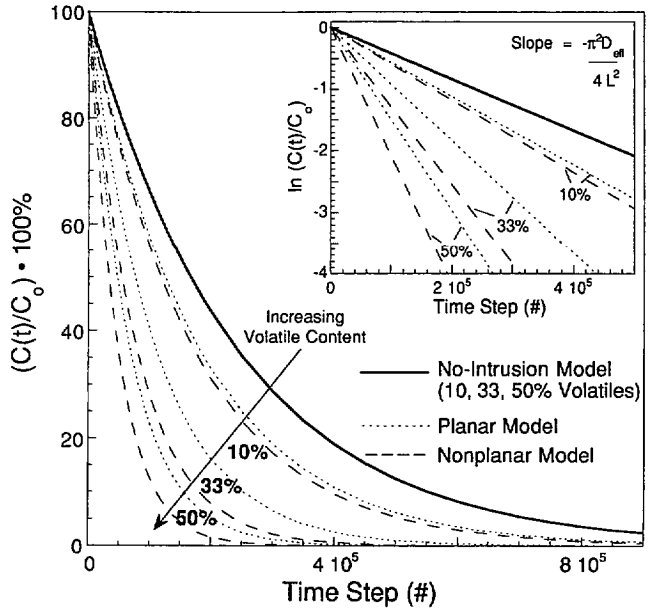

Fig. 2. Plot of the volatile (plasticizer) concentration as a function of time for each initial binder composition in the 2-D model systems (400 × 200 pixels, PD = 13 pixels) for the no-intrusion, planar, and nonplanar models. (Note: Inset depicts semilog plot of $C(t)/C_0$ as a function of time for the same systems.)

mer (nonvolatile) phase. A continuously falling rate of removal was observed in all simulation experiments, where the normalized concentration ($C(t)/C_0$) was found to exhibit an exponential time dependence, as shown in the inset of Fig. 2. The removal times were essentially independent (variations ≤8%) of the initial volatile concentration in the no-intrusion model, as expected for Fickian diffusion.[26] Thus, we chose to plot the no-intrusion $C(t)/C_0$ data as a single bold curve in Fig. 2. In contrast, the removal times decreased with increasing volatile content in both the nonplanar and planar pore development models.

The total number of time steps required to eliminate 99% of the initial plasticizer (volatile) species from the 2-D systems (400 × Z pixels, where Z = 200, 400, 600, or 800 pixels; PD = 13 pixels) with an initial volatile content of 50% is shown in Fig. 3(a). For each computer model used, the time required to eliminate the volatile species from the system increased with increasing system depth, with the no-intrusion and planar models exhibiting stronger dependencies relative to the nonplanar model. In addition, for a given 2-D system size (i.e., 400 × 200 or 800 × 400 pixels) with an initial volatile content of 50%, the time required to eliminate 99% of the volatile species from this system was found to decrease linearly with increasing particle size, as shown in Fig. 3(b). The results shown in Fig. 3(b) correspond to data obtained using the nonplanar model; however, analogous trends with stronger dependence were observed using the planar and no-intrusion models.

The differences in pore development between the nonplanar, planar, and no-intrusion models lead to varying binder removal times, as illustrated in Figs. 2 and 3(a). The resulting pore development at intermittent points during removal is shown in Figs. 4 and 5 for representative 2-D systems (400 × 200 pixels, initial volatile content = 50%, and PD = 13 pixels) using the nonplanar and planar models, respectively. In both models, porosity develops as removal progresses, leading to a reduction in the length scale for volatile diffusion relative to that found in the no-intrusion model, where the length scale equals the maximum system depth (e.g., Z = 200 pixels). The pore development is depicted by the shaded gray regions in Figs. 4 and 5. In the nonplanar model, the pore front penetrates nonuniformly into the system, advancing first through the largest pore channels (refer to Fig. 4). In the planar model, the pore front penetrates uniformly into the system by advancing a unit depth interval of one pixel as removal progresses (refer to Fig. 5).

The pore development differences described above also lead to differences in the normalized concentration profiles, $C(z)/C_0$, of volatile species as a function of depth (z), as shown in Figs. 6(a–c). The results shown in Fig. 6 represent individual simulations carried out on 2-D systems (400 × 200 pixels, initial volatile content = 50%, and PD = 13 pixels) using the nonplanar, planar, and no-intrusion models, respectively, where $C(z)$ equals the number of plasticizer species at a given depth, z. The nonplanar model produces the most uniform distribution of volatile species within the system at any given time step, where volatile concentration is zero at the top surface (z = 0) and gradually increases with increasing depth. As removal progresses, $C(z)$ at a given depth (z) decreases. In contrast, as removal progresses in the planar model, the depth (z) at which the volatile concentration is zero continuously advances into

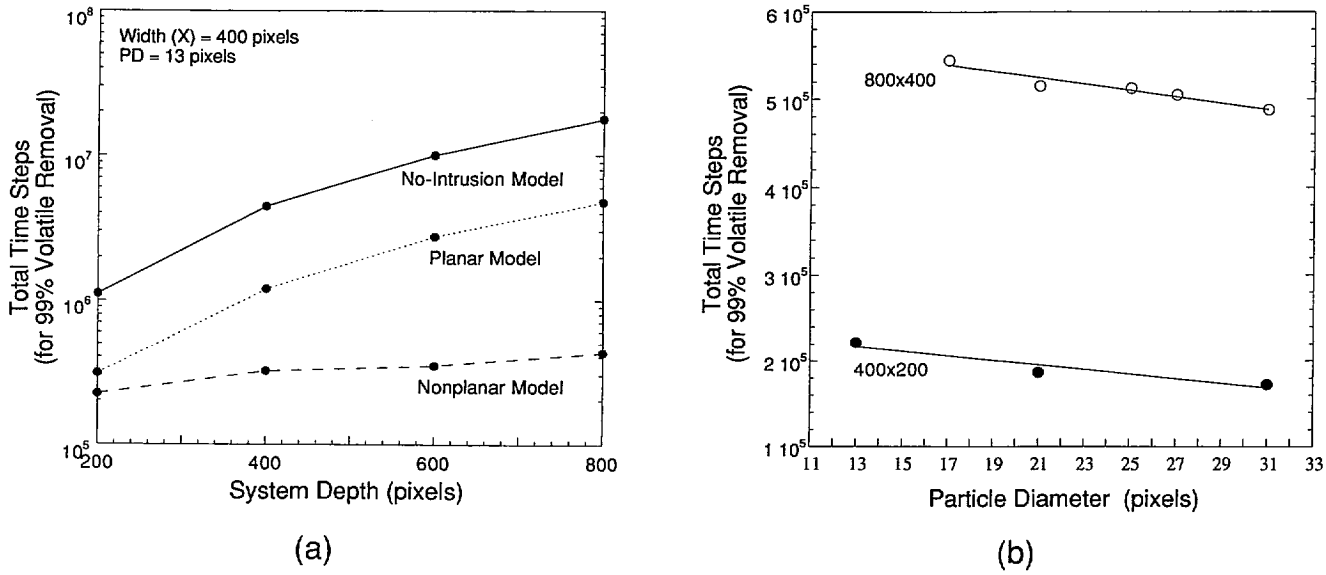

Fig. 3. Total number of time steps required for 99% removal of the volatile species from 2-D systems with 50% initial volatile content as a function of (a) system depth, and (b) particle size.

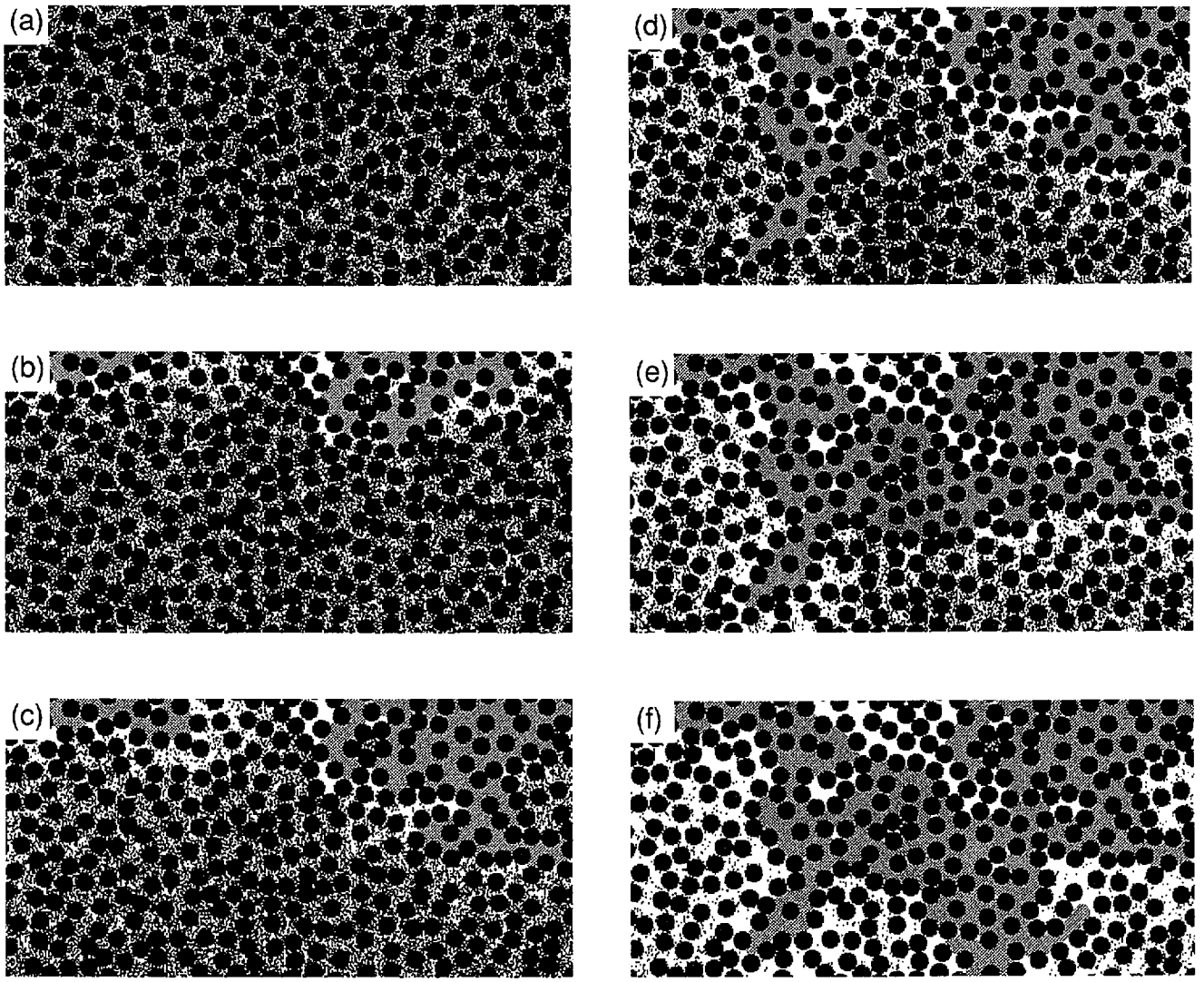

Fig. 4. Series of digitized images of a 2-D model system (400 × 200 pixels, initial volatile content = 50%, and PD = 13 pixels) at intermediate points during the removal process using the nonplanar model: (a) plasticizer concentration $C(t)/C_0 \cdot 100\% = 100\%$ (initial system), (b) $C(t)/C_0 \cdot 100\% = 80\%$, (c) $C(t)/C_0 \cdot 100\% = 60\%$, (d) $C(t)/C_0 \cdot 100\% = 40\%$, (e) $C(t)/C_0 \cdot 100\% = 20\%$, and (f) $C(t)/C_0 \cdot 100\% = 5\%$. [Color key: red = ceramic particles, blue = volatile (plasticizer) species, white = nonvolatile (polymeric) species, and gray = porosity.]

the system (refer to Fig. 6(b)). This progression leads to the greatest nonuniformity in binder distribution within the 2-D model particulate bodies (refer to Fig. 5). Finally, in the no-intrusion model, the concentration profile of volatile species develops as expected for a process where the binder–vapor interface remains pinned at the top surface ($z = 0$) at all times.

Differences in pore development also impact the binder–vapor interfacial growth observed during volatile removal from these model 2-D particulate bodies. In the nonplanar model, the binder–vapor interface grows as removal progresses because of nonuniform pore development (refer to Fig. 4). The growth of this interface, normalized as $A_{int}(t)/A_{int}(0)$, is shown as a function of time in Fig. 7 for representative 2-D systems (400 × 200) with varying particle size and initial volatile concentrations. These curves are data obtained from individual simulation runs, but are representative of the set of data collected for a given system. The value of $A_{int}(t)/A_{int}(0)$ plateaus at long times for each curve, as denoted by arrow markers in Fig. 7. The amount of interfacial growth depends on the total porosity developed as well as on the pore size distribution present in these systems. For example, the interfacial growth was more extensive with increasing volatile concentration (i.e., higher pore content) at a constant particle size. Similarly, the interfacial growth was also more extensive with decreasing particle size at a constant volatile content. The decrease in particle size produces systems with relatively smaller pore channels and, thus, a greater number of pores develop for a fixed amount of removal. As one might expect, the binder–vapor interfacial growth is also dependent upon the system size. For example, for 2-D systems (400 × Z pixels, where Z = 200, 400, 600, or 800 pixels) with a fixed particle size (PD = 13 pixels) and initial volatile content of 50%, the plateau values of $A_{int}(t)/A_{int}(0)$ increase with increasing system depth, as shown in the inset of Fig. 7. In contrast, the binder–vapor interface remains constant in the no-intrusion model, and nearly constant in the planar model. In the latter case, slight variations may arise during removal due to differences in the particle packing fraction as a function of depth (z) in these systems. However, the average binder–vapor interfacial length should deviate little from its initial value over time.

(2) 3-D Simulations

The normalized plasticizer concentration ($C(t)/C_0$) is plotted as a function of removal time in Fig. 8 for the 3-D model systems (400 × 400 × 200 pixels, PD = 13 pixels, 33% volatiles), where $C(t)$ equals the total number of plasticizer

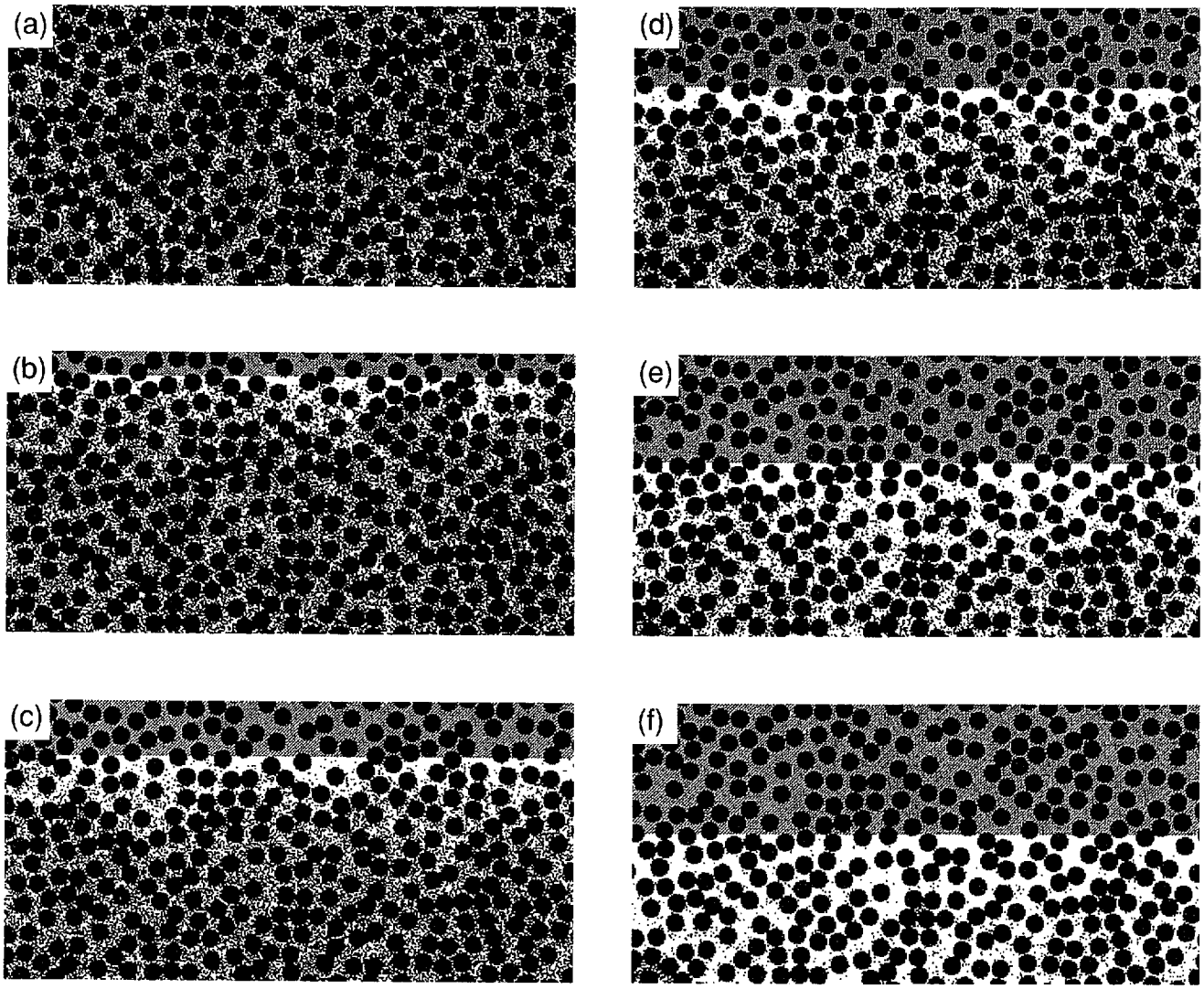

Fig. 5. Series of digitized images of a 2-D model system (400 × 200 pixels, initial volatile content = 50%, and PD = 13 pixels) at intermediate points during the removal process using the planar model: (a) plasticizer concentration $C(t)/C_0 \cdot 100\% = 100\%$ (initial system), (b) $C(t)/C_0 \cdot 100\% = 80\%$, (c) $C(t)/C_0 \cdot 100\% = 60\%$, (d) $C(t)/C_0 \cdot 100\% = 40\%$, (e) $C(t)/C_0 \cdot 100\% = 20\%$, and (f) $C(t)/C_0 \cdot 100\% = 5\%$. [Color key: red = ceramic particles, blue = volatile (plasticizer) species, white = nonvolatile (polymeric) species, and gray = porosity.]

species in the system at a given time, t, and C_0 equals the initial number of plasticizer species in the system. Again, these curves correspond to isothermal weight loss profiles for binder removal at some temperature below the decomposition temperature of the polymer (nonvolatile) phase. A continuously falling rate of removal was observed only in the planar and no-intrusion simulation experiments, where the normalized concentration ($C(t)/C_0$) was found to exhibit an exponential time dependence analogous to the corresponding 2-D cases. In contrast to the 2-D results, however, a constant rate of plasticizer removal was observed for the nonplanar simulations over a significant fraction of the removal process as highlighted in Fig. 8. It should be noted that the 3-D nonplanar removal times are over an order of magnitude lower than those observed for the corresponding 2-D systems (refer to Fig. 2). Such differences are a manifestation of the significant percolative differences between pore networks present in the 2-D and 3-D model particulate bodies. However, the normalized concentration depth profiles, $C(z)/C_0$, of volatile species in these 3-D systems exhibited features similar to those shown in Fig. 6, with the nonplanar model yielding the most uniform binder distribution during removal.

The binder–vapor interfacial growth as a function of time is shown in Fig. 9 for nonplanar removal from an individual 3-D system (400 × 400 × 200 pixels, PD = 13 pixels, 50% volatiles). Extensive growth of this interface was observed in the 3-D case. In comparison, the inset of Fig. 9 depicts the interfacial growth for a 2-D system (400 × 200 pixels) with analogously sized particles and initial volatile content. As expected, the large increase in system size with increasing dimensionality leads to substantial differences in the development of the binder–vapor interface during the removal process.

IV. Discussion

The exponential time dependence of the normalized plasticizer concentration ($C(t)/C_0$) in the 2-D systems during removal (refer to inset of Fig. 2) can be analyzed theoretically to determine the controlling distance, or effective length scale, over which diffusion occurs in the binder-filled pores. The volatile concentration, $C(t)$, at a given time, t, can be determined by carrying out a separation of variables, then integrating out the spatial dependence which yields the expression[25,26]

$$\frac{C(t)}{C_0} = \frac{8}{\pi^2} \sum_{j=0}^{\infty} \frac{1}{(2j+1)^2} \exp\left(\frac{-(2j+1)^2 \pi^2 D_{\text{eff}} t}{4l^2}\right) \qquad (2)$$

where $C(t)$ and C_0 have been previously defined, D_{eff} is the effective diffusivity, and l is the system depth. The power series solution given in Eq. (2) is valid at all times for the no-intrusion

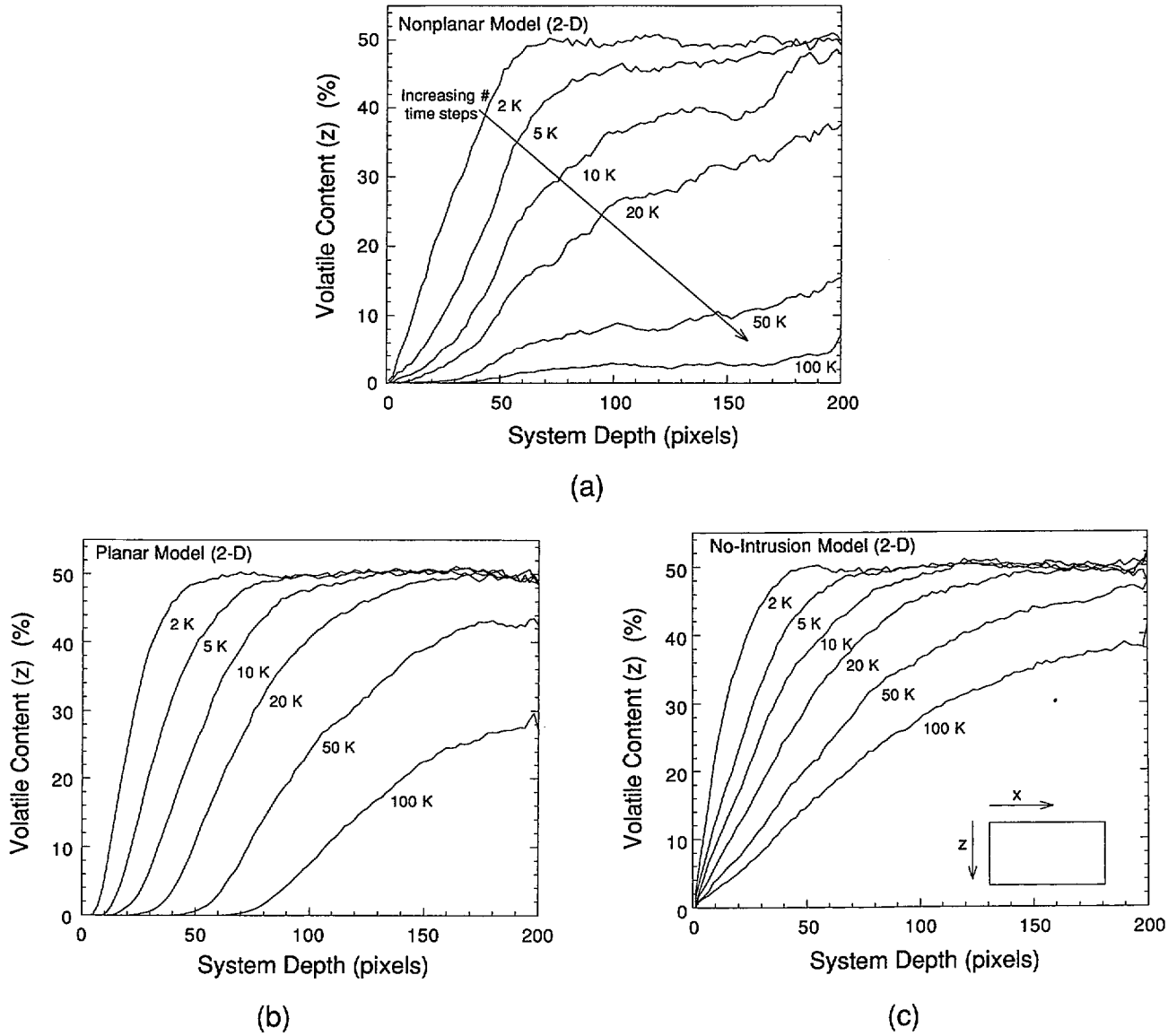

Fig. 6. Volatile concentration profiles ($C(z)/C_0$) at intermediate time steps as a function of depth (z) in the 2-D systems (400 × 200 pixels, PD = 13 pixels, and initial volatile content = 50% for (a) nonplanar, (b) planar, and (c) no-intrusion models. (Note: Intermittent time values shown for each curve are given in units of 1 K, where 1 K = 1000 steps.)

model, and can also be used to estimate an effective diffusion length (L) in the nonplanar and planar models. The first-term approximation, valid between $0 < C(t)/C_0 < 0.8$, is a particularly useful form of the above expression and is given by

$$\frac{C(t)}{C_0} = \frac{8}{\pi^2}\exp\left(\frac{-\pi^2 D_{\text{eff}} t}{4l^2}\right) \tag{3}$$

In our analysis, the effective diffusivity term in Eqs. (2) and (3) accounts for the influence of the ceramic phase and resulting pore structure on plasticizer diffusion as given by

$$D_{\text{eff}} = \frac{D_v(1 - \phi_{\text{solid}})}{\tau} \tag{4}$$

where D_v is the volatile diffusivity in the pure binder phase ($\phi_{\text{solid}} = 0$), the quantity $1 - \phi_{\text{solid}}$ is the initial binder-filled pore fraction or ε, and τ is the tortuousity factor.[27] The volatile diffusivity, D_v, was determined using the no-intrusion model for a 2-D system (400 × 200 pixels) without ceramic particles. All pixels in the system were initially assigned to the binder phase, and of these 10% were randomly assigned to be volatile species. The volatile concentration ($C(t)$) was then monitored at each time step during the removal process. A direct comparison of the volatile diffusivities calculated from Eq. (3) using results obtained from the no-intrusion model (in the absence and presence of the solid particles) yields values of the tortuousity factor, since l and ε are known quantities for these 2-D systems (i.e., l = 200 pixels and ε = 1 or 0.47 for solid contents of 0% or 53%, respectively). As an example, the tortuousity factor (τ) was found to be 1.6 and 1.2 for systems containing solid particles of diameter equal to 13 and 21 pixels, respectively. As expected, the tortuousity factor increased with decreasing particle size. Garnett[32] has determined an upper bound for the effective diffusivity ($D_{\text{eff}}^{\text{up}}$) for a two-component, 2-D medium containing "porous" and "nonporous" components as given by

$$D_{\text{eff}}^{\text{up}}(\phi_{\text{solid}}) = \left[\frac{(1 - \phi_{\text{solid}})}{1 + \phi_{\text{solid}}}\right] D_v \tag{5}$$

where ϕ_{solid} is the nonporous (or solid) fraction. Using Eq. (5), one calculates a value of 1.53 for the tortuosity factor ($=1 + \phi_{\text{solids}}$) of a two-component, 2-D system where ϕ_{solid} equals 0.53. This value is in reasonable agreement with the values given above for 2-D systems with particles of diameter 13 and 21 pixels, respectively. Since D_{eff} depends only on the

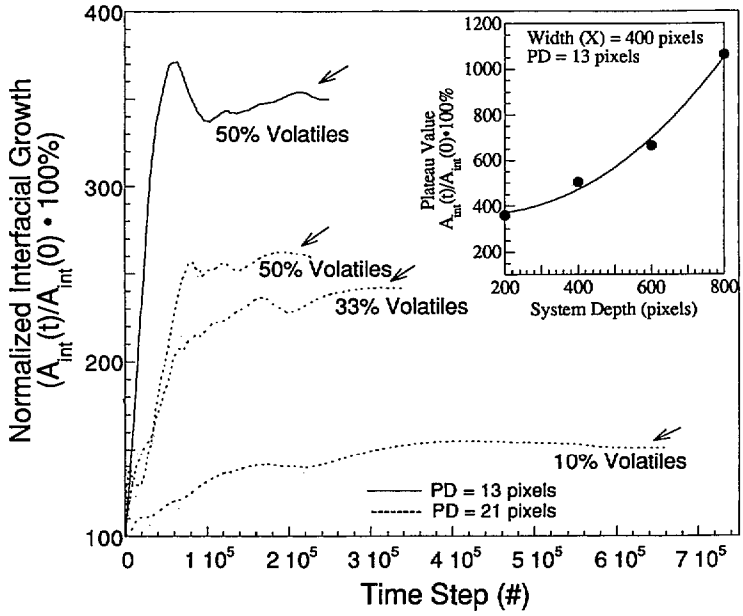

Fig. 7. Plot of the normalized binder–vapor interface growth, $(A_{int}(t)/A_{int}(0))\cdot 100\%$, as a function of time in the 2-D systems (400 × 200 pixels, PD = 13 and 21 pixels) with different initial volatile concentrations using the nonplanar model. [Note: Arrows indicate plateau values of each curve. Inset depicts the dependence of the plateau value of interfacial growth on system depth for systems of constant width (X = 400 pixels) and particle size (PD = 13 pixels).]

parameters given in Eq. (4), it is invariant for 2-D systems with constant particle size (PD) and solids loading, irrespective of system size ($X \times Z$). Furthermore, as pore development proceeds in the nonplanar and planar models, it should remain constant in those regions ahead of the binder–vapor interface where binder remains. Since the diffusing species are eliminated from the system upon reaching this interface, only the binder-filled regions influence mass transport processes in these models. Therefore, Eq. (3) should provide a reasonable estimate of the controlling diffusion distance in each of the simulation experiments.

The effective length (L) for volatile diffusion for 2-D model systems (400 × 200 pixels, PD = 13 pixels) was obtained from the slopes of the curves shown in the inset of Fig. 2, where the slope ($=-\pi^2 D_{eff}/4L^2$) of each curve is given by Eq. (3). A least-squares analysis was performed on each curve to determine their respective slopes. All curves exhibited a linear fit with a correlation factor, R, above 0.99. These slopes are plotted in Fig. 10 as a function of initial volatile content for the nonplanar, planar, and no-intrusion models. For comparison, the slopes obtained from 2-D model systems of a different particle size (PD = 21 pixels) are also shown in Fig. 10. For a given volatile concentration, the slopes are lower for systems that contain smaller solid particles due to their impact on the tortuousity factor (τ). This results in the trend shown in Fig. 3(b),

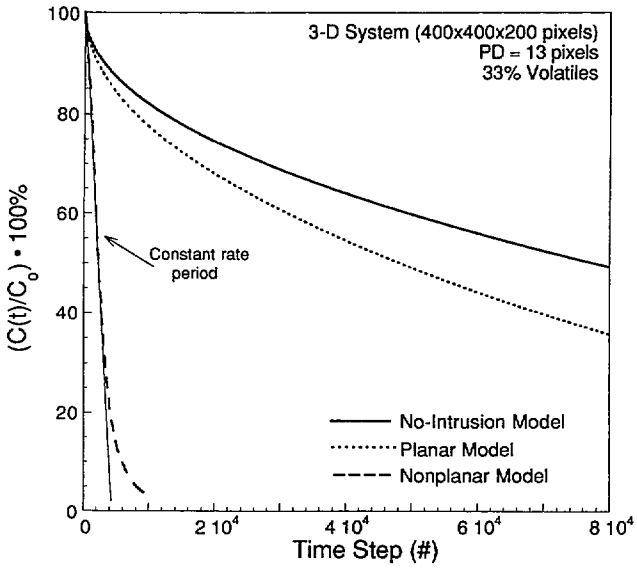

Fig. 8. Plot of the volatile (plasticizer) concentration as a function of time for each binder composition in the 3-D model systems (400 × 400 × 200 pixels, PD = 13 pixels, and initial volatile content = 33%) for the no-intrusion, planar, and nonplanar models.

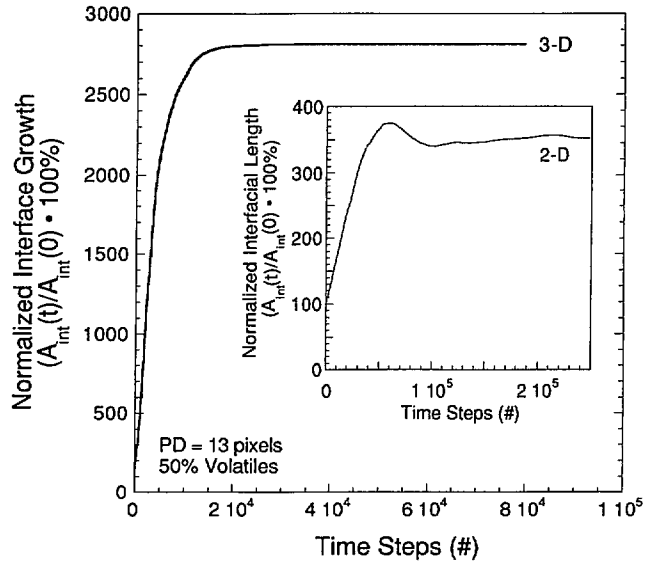

Fig. 9. Plot of the normalized binder–vapor interface growth, $(A_{int}(t)/A_{int}(0))\cdot 100\%$, as a function of time in 3-D systems (400 × 400 × 200 pixels, PD = 13 pixels) with an initial volatile content of 50% using the nonplanar model. [Note: Inset depicts the interfacial growth of the corresponding 2-D system (400 × 200 pixels, PD = 13 pixels, and initial volatile content = 50%).]

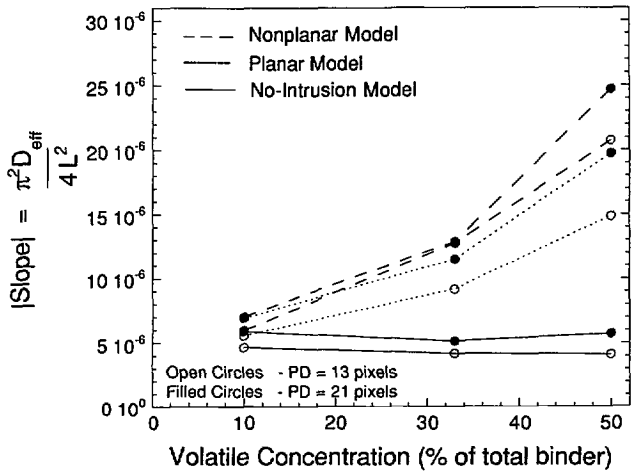

Fig. 10. Comparison of the slopes ($=-\pi^2 D_{eff}/4L^2$) of the curves shown in Fig. 2 and those obtained for 2-D systems (400 × 200 pixels, PD = 21 pixels) illustrating the dependence of the removal kinetics on the initial volatile concentration, pore development, and particle size for the nonplanar, planar, and no-intrusion models.

where the total removal time decreases with increasing particle size.

The effective diffusion length calculated from Eq. (3) as a function of initial volatile concentration is shown in Fig. 11 for 2-D systems (PD = 13 pixels) using the nonplanar, planar, and no-intrusion models. For a given volatile concentration, the nonplanar model always yielded the lowest effective length for volatile diffusion. Extensive pore development, as defined by the percolation of large pores from the top to bottom surfaces in these 2-D systems, was only observed for the highest initial volatile contents probed in this work (e.g., 50%; refer to Figs. 4(e) and (f)). Under these conditions, $L_{nonplanar}$ corresponds to the distance between the individual advancing pores (refer to Fig. 4), or roughly several particle diameters in length. Thus, $L_{nonplanar}$ is parallel to the top surface of these systems and should be relatively insensitive to system depth (Z). $L_{nonplanar}$ depends mainly on particle size, on local particle packing variations which determine the spacing between the largest pores in the system, and on initial volatile content for a given solids loading. In contrast, both L_{planar} and $L_{no\text{-}intrusion}$ depend on the system depth (Z, or the controlling geometric dimension of the simulated real ceramic component). L_{planar} scales roughly with the system depth via the following relationship: $L_{planar} \approx (1 - V_f)Z$, where V_f = initial volume fraction of volatile species in the binder phase and Z is the maximum system depth in pixels. $L_{no\text{-}intrusion}$ is simply equal to Z. In these cases, the controlling volatile diffusion distance remains perpendicular to the top surface of the 2-D systems.

The respective dependencies of $L_{nonplanar}$, L_{planar}, and $L_{no\text{-}intrusion}$ on system depth (Z) are illustrated in Fig. 12 for 2-D systems of constant width, particle diameter, and initial volatile content (where X = 400 pixels, PD = 13 pixels, and V_f = 0.5). While both L_{planar} and $L_{no\text{-}intrusion}$ are observed to increase with increasing system depth, $L_{nonplanar}$ appears to be relatively insensitive to this parameter. $L_{nonplanar}$ varies between approximately 7 to 10 particle diameters in length for 2-D systems with Y = 200 and 800 pixels, respectively. In addition, the normalized value of ΔL, where $\Delta L = (Z - L_{nonplanar})/Z$, increases with increasing system depth (refer to Fig. 12). Therefore, the reduction in binder removal times observed using the nonplanar model relative to that observed using the planar and no-intrusion models increases with increasing system size. In real ceramic components, the average ceramic particle size is normally much smaller than the component size. This is true even in tape-cast ceramic thick films which are typically referred to as 2-D components. For example, the average ceramic particle size is roughly 0.5% of the controlling geometric dimension in individual tape-cast layers (thickness = 100 μm) which contain 0.5 μm particles. This value is about an order of magnitude (or more) lower than those representative of the 2-D model systems generated in this study. Thus, one can expect actual ΔL values to be even larger than those found in our largest 2-D systems (e.g., 400 × 800 pixels with PD = 13 pixels), suggesting that capillary redistribution of the binder phase will lead to even greater improvements in real debinding times. A thorough analysis will also be carried out for the 3-D systems, when further data are obtained. However, similar trends are expected for such systems as evidenced by the substantial reduction in volatile removal times between the nonplanar and planar/no-intrusion models shown in Fig. 8.

It is noteworthy that the $C(t)/C_0$ curves for all models exhibited a continuously falling rate of volatile removal over time in the 2-D systems (refer to Fig. 2). In contrast, the nonplanar curves were found to exhibit a constant-rate period of volatile (plasticizer) removal during a significant fraction of this process in the 3-D systems (refer to Fig. 8). These 3-D results are in excellent agreement with the experimental observations

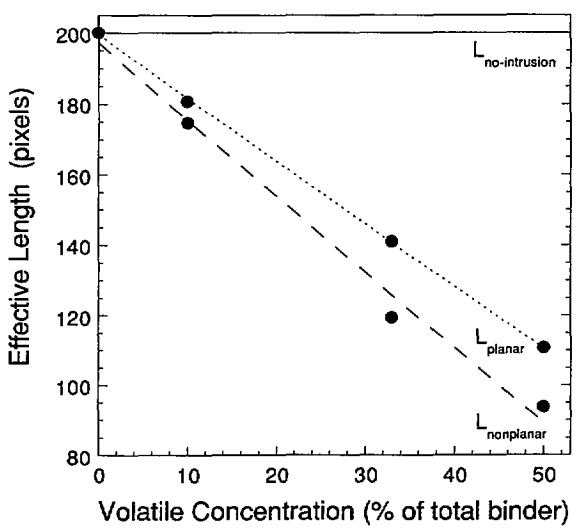

Fig. 11. Plot of the effective diffusion length, L (pixels), as a function of initial volatile concentration for the 2-D systems (PD = 13 and 21 pixels) for the nonplanar, planar, and no-intrusion models.

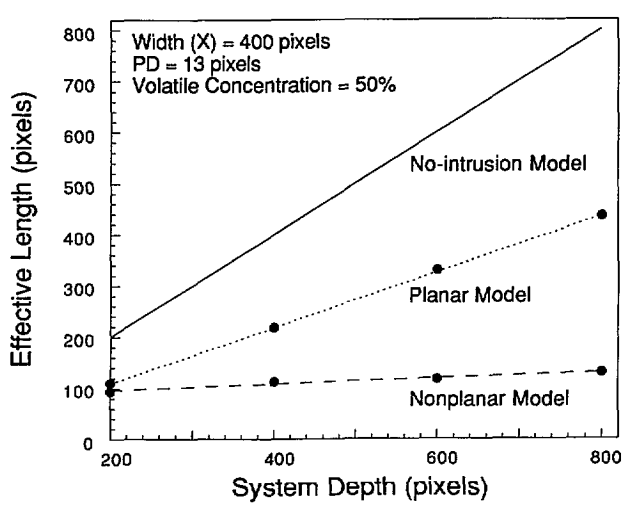

Fig. 12. Plot of the effective diffusion length, L (pixels), as a function of system depth (Z) for 2-D systems (width (X) = 400 pixels, PD = 13 pixels, and initial volatile content = 50%) for the nonplanar, planar, and no-intrusion models.

reported by Lewis and Cima,[10] which revealed the existence of a constant-rate period of plasticizer removal from ceramic tape-cast layers containing a graded-volatility, multicomponent binder system under isothermal conditions ($T < T_d$). Constant-rate mass loss requires only that the controlling resistance to mass transfer remain constant during the removal process. For example, during drying, the constant controlling resistance is often the boundary layer external to the body for evaporation of single-component systems providing the surface can be adequately resupplied with the evaporating species. In such cases, the characteristic diffusion distance remains constant in this boundary layer as long as the external conditions remain unchanged. Alternatively, for removal of volatile species from a multicomponent, graded volatility binder system, the constant controlling resistance has been attributed[9] to the distance between large penetrating pores (refer to Fig. 4) when capillary redistribution of the binder phase occurs. The lack of steady-state behavior in the 2-D nonplanar simulations is attributed primarily to system size effects. For example, one finds the spacing between large pores to be approximately 25% of the total system width (X) for 2-D systems (where $X = 400$ pixels) that contained particles 13 pixels in diameter. Such size limitations are likely to prevent the observation of steady-state behavior, because a constant length scale for mass transport is never fully established.

Our results clearly show that capillary redistribution of the binder phase during removal leads to significant reductions in removal times. However, we have assumed that binder redistribution processes occur instantaneously in this case. This assumption, valid for most drying processes, may not always be suitable for binder removal processes because of the relatively high viscosity of many multicomponent binders. In support of this assumption we refer to direct observations[10] made on commercial binder systems, such as dibutyl phthalate (33%)-plasticized PVB with an apparent viscosity on the order of 10^5 P at $T = 100°C$[10,11] which show that these systems do redistribute in porous networks in real time at elevated temperatures.[5] To assess the validity of the nonplanar model and its assumptions for a given binder system, one can use expressions (see, for example, Ref. 9) which have been developed to calculate the length scale over which capillary forces act on the binder phase based on its properties and those of the ceramic body. One would expect this assumption to be reasonable (and, hence, the model valid) when this calculated length scale is greater than the component dimensions of interest.

V. Conclusions

A series of computer simulations have been carried out to investigate the removal of multicomponent, thermoplastic binder systems fron 2-D and 3-D model particulate bodies. Simulations were performed under isothermal conditions using different pore development algorithms to study the influence of capillary-driven binder redistribution on mass transport kinetics. Several insights into the fundamental physical processes that occur during multicomponent binder removal were derived from this study. First, the simulation models enabled direct visualization of mass transport at the microscopic level during thermolysis. Additionally, key parameters were quantified including removal times, volatile concentration profiles (both cumulative and depth profiles), and binder–vapor interfacial development using these simulation models. In both the 2-D and 3-D systems, the removal times were found to dramatically depend on the pore development processes such that reductions, an order of magnitude or larger, were observed when capillary redistribution of the binder phase was permitted. In this case, the controlling length scale for diffusion depends on the initial volatile content which determines the extent of pore development, and on the spacing between large penetrating pores. Most importantly, in this case, the controlling length scale for diffusion was shown to be relatively insensitive to the system size (i.e., component geometry). With increasing system dimensionality, the characteristic removal times were observed to decrease even further for a similar set of conditions when capillary redistribution was permitted because of the large percolative differences between pore networks present in the 2-D and 3-D model particulate systems. Clearly, the optimization of industrial debinding cycles hinges critically on minimizing the controlling length scale(s) over which mass transport occurs. Our study highlights the importance of binder composition (volatile content) and capillary-driven redistribution as two key design parameters.

Acknowledgments: We gratefully acknowledge E. J. Garboczi and N. Martys (NIST), and J. Kieffer (UIUC), who have contributed to this work through several fruitful discussions. M. Galler would like to thank the Building Materials Division of the National Institute of Standards and Technology (NIST) for the use of NIST facilities during his stay as a guest researcher.

References

[1]N. A. J. Platzer, Advances in Chemistry Series, Vol. 48, *Plasticization and Plasticizer Processes*. American Chemical Society, Washington, DC, 1965.

[2]D. W. Sproson and G. L. Messing, "Organic Binder Removal Processes in Closed-Pore Organic-Powder Compacts"; pp. 528–37 in Ceramic Transactions, Vol. 1, *Ceramic Powder Science II*, Proceedings of the First International Conference on Ceramic Powder Processing Science. Edited by G. L. Messing, E. R. Fuller, and H. Hausner. American Ceramic Society, Westerville, OH, 1988.

[3]R. E. Mistler, D. J. Shanefield, and R. B. Bunk, "Tape Casting of Ceramics"; pp. 441–8 in *Ceramic Processing Before Firing*. Edited by G. Y. Onoda and L. L. Hench. Wiley, New York, 1978.

[4]M. Barone and J. C. Ulciny, "Liquid-Phase Transport During Removal of Organic Binders in Injection-Molded Ceramics," *J. Am. Ceram. Soc.*, **73** [11] 3323–33 (1990).

[5]J. A. Lewis and M. J. Cima, "Direct Observation of Binder Distribution Processes in 2-D Porous Networks During Thermolysis"; pp. 583–90 in Ceramic Transactions, Vol. 12, *Ceramic Powder Science III*. Edited by G. L. Messing, S. Hirano, and H. Hausner. American Ceramic Society, Westerville, OH, 1990.

[6]C. Dong and H. K. Bowen, "Hot-Stage Study of Bubble Formation During Binder Burnout," *J. Am. Ceram. Soc.*, **72** [6] 1082–87 (1989).

[7]P. Calvert and M. Cima, "Theoretical Models for Binder Burnout," *J. Am. Ceram. Soc.*, **73** [3] 575–79 (1990).

[8]R. M. German, "Theory of Thermal Debinding," *Int. J. Powder Metall.*, **23** [4] 237–45 (1987).

[9]M. J. Cima, J. A. Lewis, and A. Devoe, "Binder Distribution in Ceramic Greenware During Thermolysis," *J. Am. Ceram. Soc.*, **72** [7] 1192–99 (1989).

[10]J. A. Lewis and M. J. Cima, "Diffusivities of Dialkyl Phthalates in Plasticized Poly(vinyl butyral): Impact on Binder Thermolysis," *J. Am. Ceram. Soc.*, **73** [9] 2702–707 (1990).

[11]J. A. Lewis and M. J. Cima, "Mass Transfer Processes During Multicomponent Binder Thermolysis"; pp. 363–70 in Materials Research Society Symposia Proceedings, Vol. 249, *Synthesis and Processing of Ceramics: Scientific Issues*. Edited by W. R. Rhine, T. M. Shaw, R. J. Gottshall, and Y. Chen. The Materials Research Society, Pittsburgh, PA, 1992.

[12]H. H. Angermann, F. K. Yang, and O. Van der Biest, "Removal of Low Molecular Weight Components during Thermal Debinding of Powder Compacts," *J. Mater. Sci.*, **27**, 2534–38 (1992).

[13]H. H. Angermann and O. Van der Biest, "Low Temperature Debinding Kinetics of Two-Component Model Systems," *Int. J. Powder Metall.*, **29** [3] 239–50 (1993).

[14]G. W. King, "Monte-Carlo Method for Solving Diffusion Problems," *Ind. Eng. Chem.*, **43** [11] 2475–77 (1951).

[15]G. E. Murch and R. J. Thorn, "Calculation of the Diffusion Correlation Factor by Monte Carlo Methods," *Philos. Mag. A*, **39** [5] 673–77 (1979).

[16]M. S. Majerus, D. S. Soong, and J. M. Prausnitz, "Experimental Measurements and Monte Carlo Simulation of Water Diffusion into Epoxy Matrices," *J. Appl. Polym. Sci.*, **29**, 2453–66 (1984).

[17]W. W. Brandt, "Monte Carlo Simulation of Simultaneous Bulk, Grain Boundary, and Surface Diffusion," *J. Chem. Phys.*, **59** [10] 5562–70 (1973).

[18]I. C. Kim and S. Torquato, "Determination of the Effective Conductivity of Heterogeneous Media by Brownian Motion Simulation," *J. Appl. Phys.*, **68** [8] 3892–903 (1990).

[19]D. P. Bentz and T. Nguyen, "Simulation of Diffusion in Pigmented Coating on Metals Using Monte Carlo Techniques," *J. Coat. Technol.*, **62** [783] 57–63 (1990).

[20]D. Wilkinson and J. F. Willemsen, "Invasion Percolation: A New Form of Percolation Theory," *J. Phys. A: Math. Gen.*, **16**, 3365–76 (1983).

[21]J. F. Willemsen, "Flow in Porous Media: Realizations of Dynamical Growth Systems," *Prog. Theor. Phys., Suppl.*, **86**, 399–405 (1986).

[22]S. R. Broadbent and J. M. Hammersley, "Percolation Processes I. Crystals and Mazes," *Proc. Cambridge Philos. Soc.*, **53**, 629 (1957).

[23]T. M. Shaw, "Drying as an Immiscible Displacement Process with Fluid Counterflow," *Phys. Rev. Lett.*, **59**, 1671–74 (1987).

[24]E. J. Garboczi and D. P. Bentz, "Digitized Simulation of Mercury Intrusion Porosimetry"; pp. 365–80 in Ceramic Transactions, Vol. 16, *Advances in Cementitious Materials*. Edited by S. Mindess. American Ceramic Society, Westerville,

OH, 1991. See also: D. P. Bentz, D. A. Quenard, V. Baroghel-Bouny, E. J. Garboczi, and H. M. Jennings, "Modelling Drying Shrinkage of Cement Paste Mortar: Part I. Structural Models from Nanometers to Millimeters," *Mater. Struct.*, in press.

[25]H. S. Carslaw and J. C. Jaeger, *Conduction of Heat in Solids*; pp. 93–130. Oxford University Press, Oxford, U.K., 1959.

[26]J. Crank and G. Park, "Methods of Measurement"; pp. 3–40 in *Diffusion in Polymers*. Edited by J. Crank and G. Park. Academic Press, New York, 1968.

[27]C. N. Satterfield, *Mass Transport in Heterogeneous Catalysis*; p. 33. MIT Press, Cambridge, MA, 1970.

[28]N. Martys and E. J. Garboczi, "Length Scales Relating the Fluid Permeability and Electrical Conductivity in Random Two-Dimensional Model Porous Media," *Phys. Rev. B*, **46** [10] 6080–90 (1992).

[29]D. H. Napper, *Polymeric Stabilization of Colloidal Dispersions*; p. 13. Academic Press, San Diego, CA, 1983.

[30]K. Ridgway and K. J. Tarbuck, "The Random Packing of Spheres," *Br. Chem. Eng.*, **12** [3] 384–88 (1967).

[31]J. Feder, *Fractals*. Plenum Press, New York, 1988.

[32]J. C. Maxwell Garnett, "Colours in Metal Glasses and in Metallic Films," *Philos. Trans. R. Soc. London*, **203**, 385 (1904). □